Neuropharmacology 73 (2013) 10–18

Contents lists available at SciVerse ScienceDirect

Neuropharmacology

journal homepage: www.elsevier.com/locate/neuropharm

High-resolution spatio-temporal bioactivity of a novel peptide revealed by optical imaging in rat orbitofrontal cortex *in vitro*: Possible implications for neurodegenerative diseases

Antoine-Scott Badin*, John Eraifej, Susan Greenfield

Department of Pharmacology, University of Oxford, Mansfield Road, Oxford OX1 3QT, United Kingdom

ARTICLE INFO

Article history:
Received 21 February 2013
Received in revised form
12 April 2013
Accepted 8 May 2013

Keywords:
Optical imaging
Field potentials
Acetylcholinesterase (AChE)
C-terminal peptide
Alzheimer's disease
α_7-Nicotinic receptor
Methyllycaconitine (MLA)
Orbitofrontal cortex
Rat brain slices

ABSTRACT

Acetylcholinesterase (AChE) is now well known to have a secondary, non-enzymatic function independent of cholinergic transmission. In the last decade, the part of the molecule responsible for this action has been identified, i.e. a 14 amino acid peptide fragment ('T14'), deriving from the C-terminus of AChE: this peptide has been shown to be bioactive in a range of preparations and to act at an allosteric site on α_7 nicotinic acetylcholine receptors (α_7-nAChRs). Of particular significance is the finding that AChE-related peptides trigger calcium-induced neurotoxicity that may be pivotal in the process of neurodegenerative diseases, such as Alzheimer's. However to date all studies have been performed on isolated cell preparations. The aim of this study was therefore to characterise the bioactivity of T14 on meso-scale *in vitro* cortical networks ('neuronal assemblies') from rat brain slices containing orbitofrontal cortex. Local field potential (LFP) recordings showed that the T14 peptide has a selective, holistic action on cortical networks in a modulatory biphasic manner i.e. predisposing excitation at concentrations of up to 1 μM, after which the trend is reversed in favour of inhibition at higher doses (>1 μM). By contrast, a scrambled variant of the T14 peptide sequence (S14), showed no significant changes in neuronal activation. Optical imaging using voltage-sensitive dyes (VSDI) corroborated the electrophysiological findings and also provided further insight into the spatial dynamics of the effects of the peptide: T14 application had a facilitatory effect i.e. increased the time-course of activation at sub-micromolar concentrations only (700 nM) without significantly affecting the spread of evoked assemblies. Moreover: co-applying T14 with the α_7-nAChR competitive antagonist methyllycaconitine (MLA) produced inhibition in activation synchrony not seen with either agent on their own, suggesting an additive inhibitory effect. In conclusion, the T14 peptide derived from AChE produced a dose-dependent biphasic modulation of cortical networks activity dependent on the α_7-nAChR: these findings should thus provide a more comprehensive insight into the immediate actions of a novel bioactive agent of high potential relevance to neurodegenerative disorders such as Alzheimer's disease.

1. Introduction

Over the past three decades, there have been no effective new treatments for neurodegenerative diseases, notably Alzheimer's disease (AD). Drugs traditionally used to tackle the symptoms of AD include AChE inhibitors such as Galanthamine and Tacrine as well as NMDA receptor antagonists such as Memantine (Pohanka, 2011): however such treatments are widely reported to have limited clinically efficiency (Scarpini et al., 2003). This lack of progress is most likely to be due to the lack of understanding of the basic mechanisms that underpin these diseases. One possibility may be that neurodegeneration is an aberrant form of development, with the pivotal signalling molecule being a 14 amino acid peptide derived from the C-terminus of AChE identified as the salient fragment for the non-cholinergic function of AChE (Greenfield and Vaux, 2002; Greenfield et al., 2008). AChE, and hence this peptide ('T14'), is expressed in all central nervous system (CNS) neurons prone to neurodegeneration, independent of cholinergic transmission: it has already been shown to be bioactive in a range of preparations (Bon and Greenfield, 2003; Day and Greenfield, 2004; Zbarsky et al., 2004). Previous research has indeed found that T14 application induces a dose-dependent calcium entry via α_7-nicotinic acetylcholine receptors (α_7-nAChRs) (Greenfield et al., 2004, 2008; Webb et al., 1996). Indeed, it has been established

* Corresponding author. Tel.: +44 01865 271626.
E-mail address: scott.badin@seh.ox.ac.uk (A.-S. Badin).

0028-3908/$ – see front matter Crown Copyright © 2013 Published by Elsevier Ltd. All rights reserved.
http://dx.doi.org/10.1016/j.neuropharm.2013.05.019

that, independent of any cholinergic mechanisms, T14 modulates the gating dynamics of α_7-nAChRs, allowing greater Ca^{2+} currents to enter neurons. Thereby presenting a new therapeutic possibility: intercepting the actions of C-terminus AChE peptides at α_7-nAChRs before sufficient neurodegeneration has taken place to trigger the emergence of symptoms.

Although two early electrophysiological studies suggested a bioactivity of the peptide (Bon and Greenfield, 2003; Greenfield et al., 2004), most of the more recent subsequent research has been undertaken in cell cultures (Bond and Greenfield, 2007; Bond et al., 2006; Onganer et al., 2006) and tissue cultures (Day and Greenfield, 2004; Emmett and Greenfield, 2004; Zbarsky et al., 2004). Moreover, an additional drawback of these approaches has been the protracted time course of the effect studied. In order to study the bioactivity of the peptide therefore on a more physiological spatial and temporal scale, i.e. with a resolution of micrometres (μm) and milliseconds (ms), the aim of this study was to monitor the immediate effects of the peptide on integral cortical networks, induced by T14 application. Such an optical imaging approach has already been shown to provide unparallelled comprehensive data about the dynamics of cortical networks in relation to bioactive compounds (Collins et al., 2007; Devonshire et al., 2010a, 2010b).

This study, however, is the first of its kind to utilise combined techniques of electrophysiology and VSDI to investigate the acute effect of T14 on cortical networks: the more established and familiar technique of field potentials provide a frame of reference for comparing the observations with optical imaging. In both types of experiments the effects of T14 were compared with those of a scrambled variant (S14) and also tested in the presence of a competitive α_7-nAChR antagonist, methyllycaconitine (MLA).

2. Methods

2.1. Brain slice preparation

Male Wistar rats (35–40 day old) were anaesthetised using isoflurane: 15 mL 100% w/w isoflurane was applied to the cotton bed at the bottom of an anaesthesia chamber (glass box 20 × 15 × 15 cm) where rats were then placed for ~45 s until anaesthesia was complete. The hind paw of each anaesthetised rat was pinched to check for appropriate depth of anaesthesia. Once the anaesthesia was confirmed, rats were quickly decapitated before immersing the brain in oxygenated ice-cold artificial cerebrospinal fluid (aCSF in mmol: 120 NaCl, 5 KCl, 20 $NaHCO_3$, 2.4 $CaCl_2$, 2 $MgSO_4$, 1.2 KH_2PO_4, 10 glucose, 6.7 HEPES salt and 3.3 HEPES acid; pH: 7.1) for 4 min, the time taken to cut the brain into slices. Coronal slices (400 μm thick) were cut from a block of brain containing prefrontal cortex (PFC; slices were taken between +12.20 and +10.70 mm Interaural and +3.20 and +1.70 mm Bregma) using a Vibratome (Leica VT1000S) and transferred to a bubbler pot containing aCSF at room temperature ('recording' aCSF in mmol: 124 NaCl, 3.7 KCl, 26 $NaHCO_3$, 2 $CaCl_2$, 1.3 $MgSO_4$, 1.3 KH_2PO_4 and 10 glucose; pH: 7.1), which was identical to that which was used during electrophysiological recordings and VSDI. Slices were left in oxygenated (95% O_2–5% CO_2) 'recording' aCSF to recuperate for at least 2 h before preparing them for electrophysiology, and 1 h before VSD staining.

2.2. Drug preparation & application

Acetylcholinesterase (AChE) C-terminus 14 amino acid peptide (T14; sequence: 'N' – AEFHRWSSYMVHWK) was custom synthesised and purchased from Genosphere Biotechnologies (Paris, France) at >99% purity, while the scrambled variant (S14; sequence: 'N' – HSWRAEVFHKYWSM), used as a positive control in this study, was custom synthesised and purchased from AnaSpec (San Jose, CA, USA) at >90% purity. All peptides were synthesised using the fmoc method, purified with HPLC and analysed using mass spectrometry. Methyllycaconitine citrate salt hydrate (MLA; Sigma–Aldrich, Saint Louis, MO, USA), the selective α_7-nAChR antagonist, was purchased from Sigma–Aldrich. All drug stock solutions were prepared prior to the start of experiments in frozen aliquots. For production of drug perfusion solutions, stock solution aliquots were thawed and added to 'recording' aCSF as appropriate and bath applied at a constant rate of 2.5 mL per min perfusion using a Minipulse 3 pump (Gilson Scientific Ltd, Bedfordshire, UK). Perfusion conditions were 32 min in duration (35 averaged frames per perfusion condition, Fig. 1C and D).

2.3. Electrophysiology

Field potential recordings (fEPSP) were acquired using GC150F-10 glass capillaries (Harvard Apparatus, Kent, UK) recording electrodes filled with 2 M NaCl solution containing 2% Pontamine sky blue 5BX dye (BDH Chemicals Ltd., Poole, England) for the electrode to be visible under the 4.5× magnification microscope (Micro Instruments Ltd, Oxford, UK). Layer I–II/III were identified with respect to distance from the pial surface and position within the ventral part of the dorsal agranular insular (AId_2) cortex, Layer V–VIa were accepted to be 500–750 μm from the position of the stimulating electrode, deep within the cortex (Van Eden and Uylings, 1985). Concentric bipolar stimulating electrodes (Frederick Haer & Co., ME, USA), with impedance (measured at 1000 Hz): 500 kΩ, were positioned within Layer II/III (since that is approximately where thalamo-cortical afferents project to stimulate cortical networks). Recording electrodes, on the other hand, were placed within Layer V–VIa, approximately 600 μm from the stimulating electrode in accordance with cytoarchitectonic studies performed in the rat PFC (Van De Werd and Uylings, 2008) in order to record the transduced, integrated neuronal response after 4–5 ms following initial stimulation; as a result, fEPSP traces showed response deflections nicely segregated from their respective stimulation artefact.

fEPSPs were amplified using an IR-283 Amplifier (Neuro Data Instruments Corp., PA, USA) coupled to a Micro 1401 mk II acquisition system (CED Ltd, Cambridge, UK) and displayed in Signal software (CED Ltd, Cambridge, UK) then saved onto the disk for off-line analysis. The IR-281 Amp was used to amplify field potential signals 1000×, so all fEPSP graphs are shown with units $\times 10^{-3}$ V. Single stimulations (14 s inter-stimulus interval – ISI) were applied to Layer II/III and the evoked responses recorded from Layer V–VIa pyramidal cell bodies with perfusion solutions being held at 30 ± 1.5 °C by a TC-202A Temperature Controller (Digitimer Research Instruments, Hertfordshire, UK) (Van De Werd and Uylings, 2008).

2.4. VSD setup

Slices were placed in a dark, high humidity chamber filled with aCSF bubbling with 95% O_2–5% CO_2. Once there, the dye solution (4% 0.2 mM styryl dye pyridinium 4-[2-[6-(dibutylamino)-2-naphthalenyl]-ethenyl]-1-(3-sulfopropyl)hydroxide (Di-4-ANEPPS, Invitrogen, Paisley, UK) (Tominaga et al., 2000) in aCSF 48%, fetal bovine serum 48%, DMSO 3.5% and cremophore EL 0.4%) was applied to the slices for 20–25 min before being transferred to an aCSF bubbler pot (room temperature, 22 ± 1.5 °C) for 1 h to wash off excess dye and recover. When starting VSD recordings, slices were placed in the recording bath on a small piece of filter paper to keep slice alive and was weighed down appropriately using a home-made plastic grid placed atop the slice. Stimulating electrodes were placed in the same location as in electrophysiology recordings (Layer II/III, ~80 μm from pial surface) with the same ISI and temperature control. For acquiring of VSD data, 16-bit images were recorded with 1 ms resolution with a digital camera (Brain Vision MiCAM Ultima R3-V20 Master) with Ultima 2004/08 imaging software (Brain Vision) coupled to Spike 2 V6.0 (CED Ltd, Cambridge, UK) which was used to trigger stimulations with respect to appropriate ISI. Light was generated using an Osram halogen xenophot 64634 HLX EFR Display/Optic lamp and was filtered to emit green (530 ± 10 nm) light using a MHF-G150LR (Moritex Corporation) coupled to MiCAM Ultima ultra-fast imaging system and filtered the emitted fluorescence through a >590 nm high-pass filter as described previously (Collins et al., 2007; Devonshire et al., 2010a, 2010b).

2.5. Data analysis and statistics

Electrophysiology experiments produced a total of 140 data traces (frames) per drug condition (32 min, 14 s ISI). Stimulations produced a large artefact which was quite distinct and separate from the region of interest of the response trace (see Supplemental Fig. 1). Using MatLab (v7.9.0.529; The MathWorks, Inc., USA), every 4 frames were averaged together to produce a total of 35 averaged frames per drug condition. The lowest point of the negative trace deflection between 4 and 7 ms after stimulation was measured for every averaged trace and plotted on axis of 'Response Amplitude' (y) vs 'Averaged Frames' (x) to produce the final electrophysiology trend graphs seen in Fig. 1 (see Supplemental Fig. 1 for methods).

VSDI produced 4 × 4 mm (100 × 100 pixels) 2-dimensional images from which critical data were extracted such as the time-course of activation and intensity of the overall elicited signal. For each VSDI experiment, each snapshot's data between 2 and 15 ms after stimulation, encapsulating the peak response (see Supplemental Fig. 1), had their parameters measured and averaged for each drug condition (total of 76 snapshots per drug condition). Such data were then compiled to produce detailed, quantitative, graphs of the extent of activation intensity as well as qualitative 'space-time' maps allowing to measure the effects of drug treatment on the spatio-temporal activation patterns of elicited neuronal assembly activation. For each experiment, the averaged data of each perfusion epoch were plotted in order to gain better knowledge of the extent to which activation intensity and time-course were affected by drug treatment. All statistical tests (paired bidirectional Analysis of Variance – ANOVA) were performed using Mathematica 8 (Wolfram Research, USA). For all statistical tests $P < 0.05$ was considered significant; data are expressed as mean ± S.E.M.

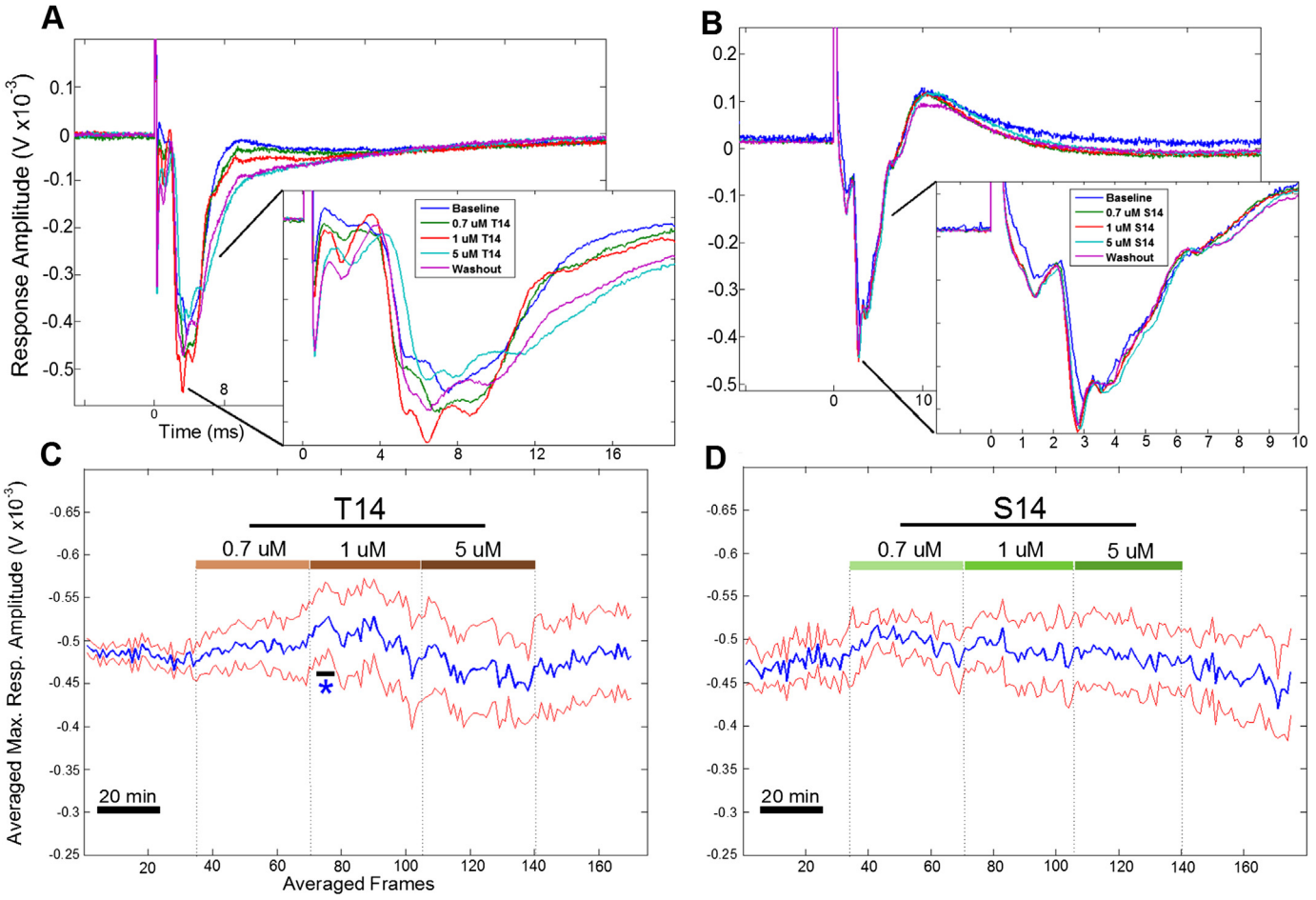

Fig. 1. Bioactivity of T14 is sequence-specific: Field potential recordings (fEPSPs) showing example traces for T14 (**A**) and S14 (**B**), and resulting fEPSP trend graphs (**C** – T14, $n = 7$; **D** – S14, $n = 6$). **C** and **D** are displayed on identical axis, while **A** and **B** are portrayed on fitting scales for individual trials, respectively. For both experiments, perfusion conditions are 32 min in length. Slices were perfused with aCSF if not indicated otherwise and stimulated between 5 and 15 V. Error bands shown in red display the standard error of the mean and stars show significant difference from baseline ($P < 0.05$). (For interpretation of the references to colour in this figure legend, the reader is referred to the web version of this article.)

3. Results

The main objective of the present study was to establish if the T14 peptide affects cortical communication during acute exposure, and if so, to characterise those pharmacological effects. Using extracellular electrophysiology, the response of cortical network activity to short T14 perfusion conditions (32 min epochs) were quantified over time at three different T14 concentrations: 0.7, 1 & 5 μM (as suggested by previous work from Bon and Greenfield, 2003). As a positive control, identical experiments were carried out using the S14 peptide: a scrambled version of the T14 (see Methods), to check if the actions of the T14 are sequence-specific or if the recorded effects are as a result of the addition of any non-specific peptide within the slice. In both cases, values from each of the 37 frames (one perfusion condition) in the baseline condition were averaged together to provide a single baseline value (T14: 0.481 ± 0.008; S14: 0.462 ± 0.007) which were then compared to segments from matching experiments' peptide treatments to check for significance. Fig. 1 shows results from the above-mentioned T14 and S14 experiments: the 0.7 μM T14 perfusion shows T14 enhances neuronal activity within the slice which is only significant for a small amount of time (~6 min) following the start of the 1 μM T14 perfusion (0.536 ± 0.025 V, 11.4 ± 5.2% increase from baseline, $n = 7$; significant – $P < 0.05$; Fig. 1C). Beyond this point, the trend inverts and an inhibitory action of the peptide is seen at higher doses, though never reaching significantly different levels from its respective baseline. Fig. 1C also shows how application of T14 dramatically increases the magnitude of the error, indicative of an induced variability in effects between T14 experiments. Fig. 1D shows the results for the S14 peptide, and though an excitatory trend is seen in the first half of the 0.7 μM epoch, at no point did this change reach a level of significant difference from baseline ($n = 6$; non-significant – $P > 0.05$; Fig. 1D), suggesting the effects of the T14 are sequence-specific. Additionally, the perfusion of increasing concentrations of S14 also shows a broadening of the error band, though this effect is seen at a much lower extent than with T14 experiments.

The enhancing actions of T14 on neuronal communication have already been linked to its actions as a positive modulator on the α_7-nicotinic acetylcholine receptor (nAChR) (Bon and Greenfield, 2003; Greenfield et al., 2004), and this may explain how its specific sequence may give rise to its bioactivity. Our following experiments were therefore carried out to test the importance of the α7-nAChR in producing the effects seen with T14 on cortical networks: MLA, a specific α7-nAChR antagonist, was used in order to interfere with this specific ACh receptor. Fig. 2A shows the lack of effects, both in affecting the mean average trace as well as in affecting the magnitude of the error, seen when perfusing slices with MLA ($n = 5$; non-significant – $P > 0.05$;) – confirming the health of our preparation as well as justifying the use of MLA as a

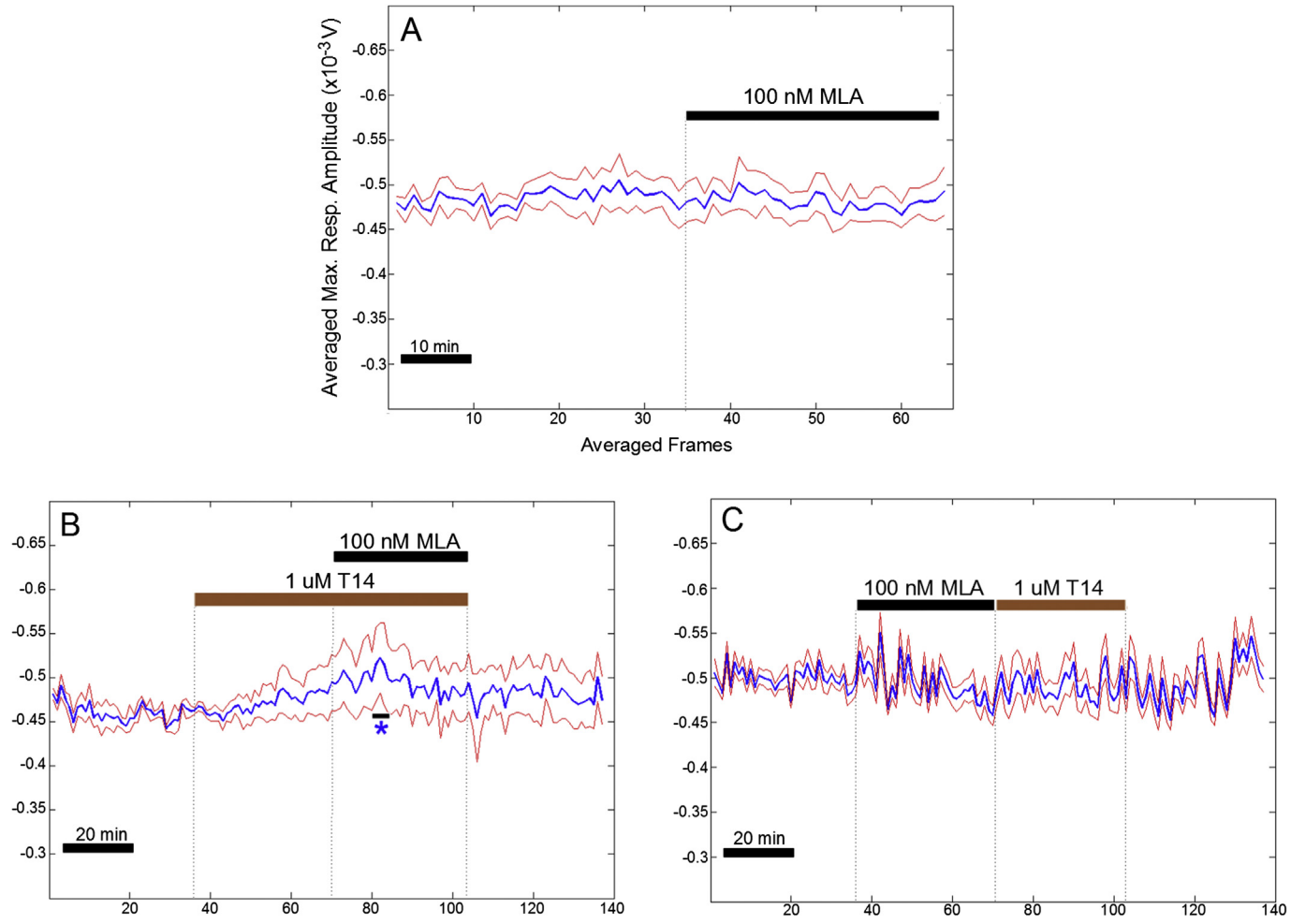

Fig. 2. MLA antagonises overall T14 effects: fEPSP recordings from MLA (**A**; $n = 5$), T14 and T14 & MLA (**B**; $n = 5$) and MLA followed by T14 (**C**; $n = 5$) experiments, shown here on identical axes. Slices were perfused with aCSF if not indicated otherwise and stimulated between 5 and 15 V. Error bands shown in red display the standard error of the mean and stars show significant difference from baseline ($P < 0.05$). (For interpretation of the references to colour in this figure legend, the reader is referred to the web version of this article.)

control antagonist. T14 experiments showed that the 1 μM epoch produced the most marked effects on cortical activity; this concentration was therefore used for all subsequent experiments. Fig. 2B shows the results from the application of T14 (1 μM) followed by the additional application of MLA: as seen previously, T14 enhances cortical activity which takes over 30 min to reach a significant deviation from baseline (average baseline value: 0.462 ± 0.007 V; significant deviation: 0.529 ± 0.03 V, 14.5 ± 6.5% increase from baseline, $n = 5$; significant – $P < 0.05$), after which the effects are stabilised and reversed back towards baseline level. Interestingly, when applying MLA first, then followed by T14, the enhancing effects of T14 were blocked ($n = 5$; non-significant – $P > 0.05$; Fig. 2C).

In addition to measuring the effects of T14 with field potentials, matching experiments were performed using VSDI to grasp a more comprehensive view of the acute effects of the peptide on the spatial parameters of propagating waves of activity ('neuronal assemblies' (Wlodarczyk et al., 2008; Wu et al., 2008)). VSDI experiments were carried out for T14 alone (0.7, 1 & 5 μM), MLA (100 nM), 1 μM T14 followed by the addition of MLA (100 nM) and MLA followed by T14: the spread of evoked propagating activity was not significantly changed by any drug treatment ($P > 0.05$ in all cases, data not shown), however the intensity of activation within those evoked assemblies was significantly decreased from baseline (as opposed to the increase in cortical output seen with field potentials) for T14 & MLA experiment (Fig. 3C) and for T14 perfusion following MLA treatment (Fig. 3D).

Fig. 3 shows a trend of enhanced activity with the T14 experiments (though non-significant; $n = 7$; $P > 0.05$) which matches to some extent results seen with field potentials. The most interesting results however come from the experiments involving T14 and MLA: in both cases (Fig. 3C and D), the third and fourth perfusion conditions (red and yellow traces respectively) showed significant decreases in intensity compared to baseline (blue trace) which lasted at least 64 min as in both cases the washout did not recuperate. Therefore when measured with VSDI, the intensity of activation of cortical networks are reduced, however only when exposed to *both* high T14 and MLA concentrations (1 μM and 100 nM respectively). Also, this decrease is seen not only during the peak response but also during the more latent return to baseline. In both cases, the intensity is reduced to a similar degree, whether the two drug treatments take place together or one after the other, suggesting a significant amount of MLA must remain active within the slice for up to half an hour after the end of its perfusion (i.e. during T14 treatment, Fig. 3D).

Fig. 4 shows sample 'space-time' maps from each of the four experiments presented in Fig. 3. These sample maps provide an effective way to assess changes to the time course of assembly activation: the longer the 'tail' after initial activation, the longer activity was sustained in cortical networks after initial stimulation.

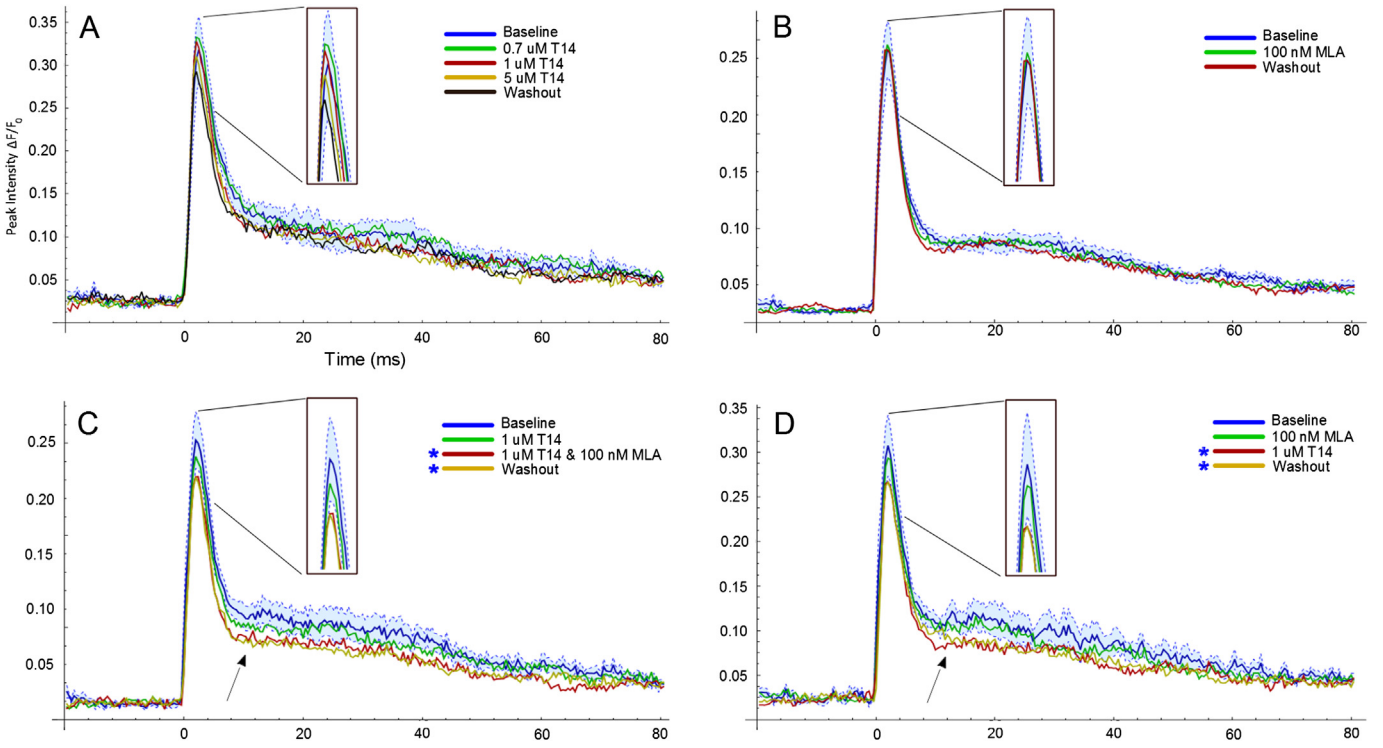

Fig. 3. Quantification of evoked assembly activation intensity as a result of drug treatment: Montage showing the time-course of maximum activation intensity over time, in response to T14 (0.7, 1 & 5 μM; $n = 7$; **A**), MLA (100 nM; $n = 6$; **B**), T14 followed by the addition of MLA ($n = 6$; **C**) and MLA then replaced with T14 ($n = 6$; **D**). Insets in each panel show a magnification of the peak response (where statistical significance was measured). Statistical significance for each trace is indicated by a star (*) in the corresponding graph's legend. Arrows show additional areas where drug condition traces were also significantly lower than baseline trace. For clarity, these graphs only show the error band (blue) for the baseline condition. (For interpretation of the references to colour in this figure legend, the reader is referred to the web version of this article.)

Fig. 4A shows that, as seen with field potentials, the application of low dose T14 increased the intensity and time-course of assembly activation, a trend that was reversed by perfusion of higher concentrations of the peptide. The use of MLA as a highly specific α_7-nAChR antagonist with presumably no off-target effects was further justified using VSDI: Fig. 3B shows identical traces for baseline, MLA and washout in terms of its quantifiable intensity – the same was true with regards to the spread of activation (data not shown). Similarly, the time-course of activation, as seen on 'space-time' maps, showed a negligible non-significant decrease as a result of MLA application compared to baseline and washout (Fig. 4B) i.e. no effect. This slight inhibitory trend is most probably attributable to the acute blockade of excitatory α_7-nAChR within the slice by MLA, and is readily reversed during washout. In this instance, when referring to 'the spread', we refer to the *overall* spread of activity within the region of interest (ROI) and over the pixel row (PR) of interest: laterally along the pial surface as well as across cortical layers. For the T14 and MLA experiments however (Fig. 4C and D), the effects of drug treatment on the time-course of assembly activation were closely correlated with effects seen on intensity of activation. Again, a marked decrease in the time-course of activation is seen in the third perfusion condition, once T14 and MLA have been co-applied to slices, and this decrease in neuronal assembly output remains for the duration of those experiments' washout perfusions. It is worthwhile to note that in the absence of drug treatment, VSDI recordings produced space-time maps that were near-identical to one another over 5 control perfusion conditions (175 min; see Supplemental Fig. 2A), confirming that all effects seen are as a result of drug treatment and not due to insults to the slice. In order to check whether co-application of T14 and MLA caused damage to the slices, as could be inferred by the prolonged reduced intensity outputs seen with VSDI, a double 'washout' perfusion (64, instead of 32 min) was carried out in one of the T14 & MLA experiments (see Supplemental Fig. 2B): the second washout perfusion showed more recovery compared to that seen during the first washout perfusion, as seen by the gradual return of yellow and light-green pixels within the activity trace. These results suggest that the reduction in neuronal activation intensity is attributable to lasting effects of T14 and MLA co-application: the effects seen are unlikely to be due artefacts related to general drug application, since they were receptor mediated (i.e. MLA-sensitive) and moreover the control peptide S14 was ineffective.

4. Discussion

The aim of the study was to examine the acute effect of the peptide derived from AChE, T14, on the meso-scale activity of cortical networks within rat brain slices. This research was conducted exploiting the reliability and temporal resolution of extracellular electrophysiology while utilising the newer technique of voltage-sensitive dye imaging to appreciate the spatial dynamics of neuronal activation in meso-scale 'assemblies' (Collins et al., 2007). Such complex activation patterns were recorded from slices containing agranular insular cortex (AId_2; part of the PFC): this part of the associative neocortex, in humans, is often among the primary target areas of neurodegeneration as seen in AD (Scahill et al., 2002), characterised by cellular shrinkage, axonal disruption and dendritic spine loss, and ultimately frank cell loss (Narr et al., 2005; Shaw et al., 2008). Research has shown that the long cortico-cortical projections and large excitatory pyramidal cells in layers III and V which make up these neuronal projections in heteromodal associations appear to be most vulnerable to degeneration seen in AD (Hof and Morrison, 2004; Morrison and Hof, 1997). This study investigated the possible initial triggering processes

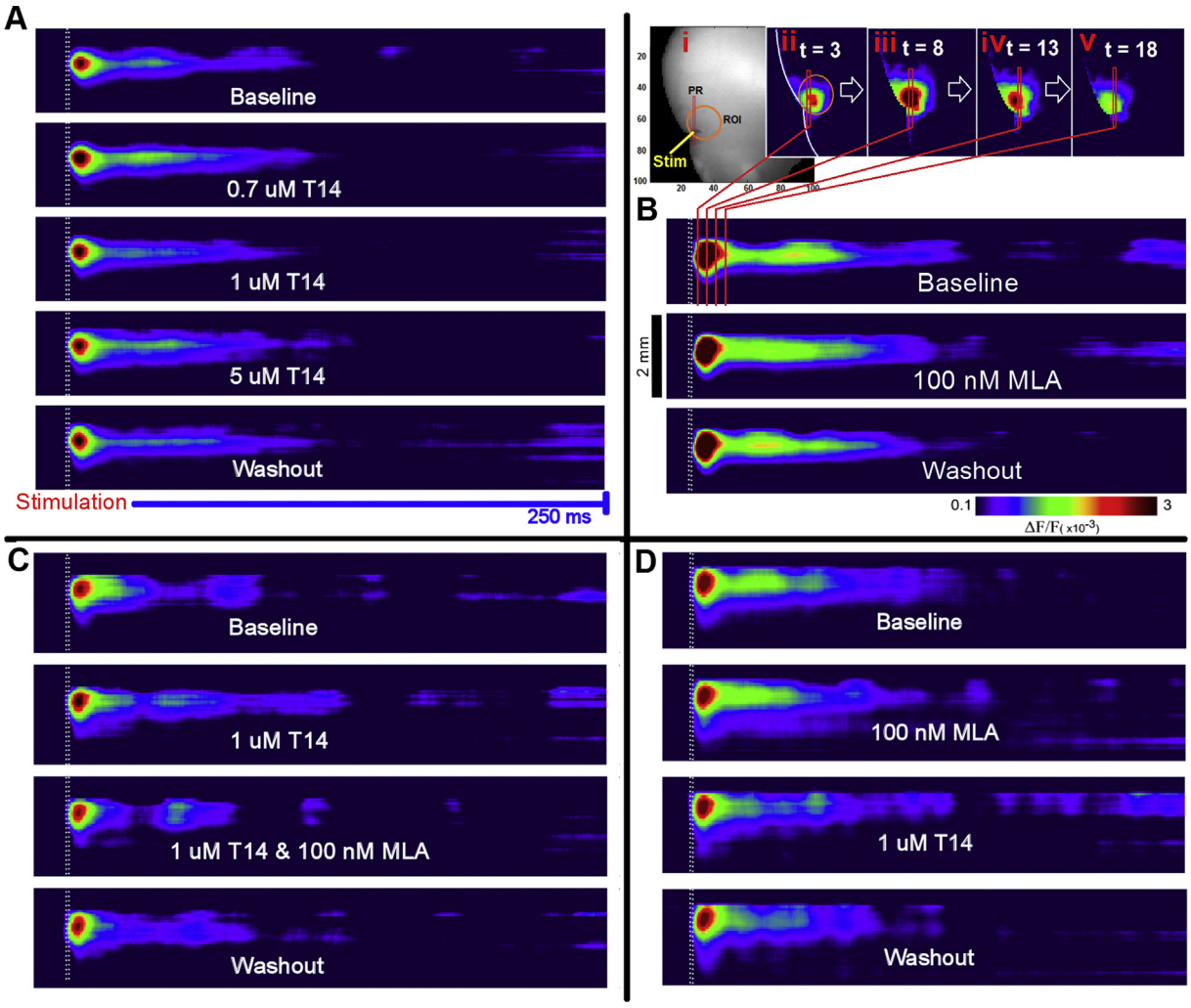

Fig. 4. 'Space-time' maps showing the time-course of evoked assembly activation: Qualitative effects of drug treatment on the time-course of assembly activation. Sample space-time maps from T14 (**A**), MLA (**B**), T14 followed by the addition of MLA (**C**) and MLA then switched to T14 (**D**) experiments are shown to illustrate the highly modulatory nature of T14's effects on cortical networks. Each panel shows the activity of a 2 mm-long row of pixels ('PR', 50 pixels in length, 1 pixel in width; each pixel is 40 μm long; **B.i.**), lying over the area of interest ('ROI'), along a 250 ms time-frame (stimulation occurs after 20 ms). Stimulation is depicted by the white dotted line seen on the space-time maps. Inset to panel **B**: **i**. Bright field view of the slice in the recording bath with electrode set in Layer II/III of the AId_2; each axis is 100 pixels (4 mm) in length. **ii**–**v**. Montage showing sequential activity of evoked responses in cortical slices at 3 (**ii**), 8 (**iii**), 13 (**iv**) and 18 (**v**) ms after initial stimulating pulse (encapsulating the peak response component), illustrating the method by which space-time maps were compiled and displayed.

induced by AChE-related peptides, at the meso-scale population level.

4.1. Why should T14 peptide be relevant to neurodegeneration?

An important clue to the basic mechanism of neurodegeneration is that a range of diseases, namely AD, Parkinson's disease, Motor neuron disease and other related disorders such as Lewy Body dementia and Guam syndrome all show a co-pathology (Aarsland et al., 1996; Gearing et al., 1995; Hulette et al., 1995). Neurodegeneration is characterised in all cases primarily by continuing neuronal death within a particular sub-population of brain cells, referred to as the 'isodendritic core' (Rossor, 1981) or 'global' systems (DeKosky, 2001; Vickers et al., 2000), due to their diffuse projection throughout the brain (Woolf, 1996). Irrespective of the transmitter used in different sub-populations, these global neurons all contain AChE which, tellingly, is secreted in a soluble form (Greenfield et al., 2008). AChE is normally released in a 'G4' conformation (4 catalytic subunits (Massoulie et al., 1999)) where these units oligomerise via a disulphide bond that includes the C-terminus containing the T14 peptide. However, only once the C-terminus is cleaved from the G4, can the salient fragment freely bind to α_7-nAChRs, while the respective AChE subunits can only now exist in the G1 form. Such a sequence of events would explain why, in both developing brains as well as in AD patients, but not for healthy adults, the G1 form dominates in the brain over the G4 (Arendt et al., 1992; Garcia-Rates et al., 2013): moreover, since the bioactive peptide itself is unlikely to remain stable indefinitely, this observation provides the strongest evidence to date, that the peptide can be present as an independent entity. Furthermore these observations suggest that AChE, through its 'global' release in the brain, acts as a modulator by virtue of the peptide fragment, at the meso-scale or population level of brain organisation.

One of the non-classical functions of AChE which may result from this in the longer term, is the activity of AChE as a trophic factor in the development of neurons as seen in the embryo/stem cells (Ling et al., 1995; Robertson and Yu, 1993; Soreq and Seidman, 2001). In an adult, global neuronal systems retain their sensitivity to growth factors (Gould et al., 1991; Oh et al., 1991) and in response to damage/oxidative stress, compensation occurs through neurite growth (Oh et al., 1991) as well as the secretion of soluble AChE (Bond et al., 2006) respectively. This neurite growth appears to

become a problem as it is aberrant, lacking the order seen in embryological development. This leads to the outgrowth of tangles of neurites in rat brain hippocampus tissue cultures (Day and Greenfield, 2004) which are characteristic of those seen in the brains of patients with AD. As a result, further understanding of the effects of the trophic peptide fragment originating from the C-terminus of AChE (the T14 and related peptides) is central to gaining further understanding of how they affect cortical networks and taking further this novel mechanistic theory of neurodegeneration.

Additionally, anti-AChE drugs (such as tacrine) have also been reported to retard the development of AD-associated beta-amyloid plaques through non-cholinergic mechanisms (Lahiri et al., 1998, 1994), corroborating the importance of non-cholinergic mechanisms demonstrated in the present study. Such a phenomenon was in fact observed in a range of experiments using ligands with structures built around a phenylcarbamate backbone (Lahiri et al., 2007; Shaw et al., 2001). The fact that AChE antagonists to some extent block the production of beta-amyloid strengthens the hypothesis that proteins admittedly involved in cholinergic transmission, such as AChE and nicotinic receptors among others, also act in separate, non-cholinergic mechanisms involved in the pathology of AD. The present study specifically highlights the possible importance of a small peptide (T14 peptide), cleaved from the C-terminus of AChE, which is shown here to interact with α_7-nAChRs in affecting the activation dynamics of meso-scale cortical networks.

4.2. T14 induces a modulatory biphasic effect on cortical network activity

T14 showed, upon application of increasing micromolar range concentrations, a biphasic modulatory effect on cortical networks within PFC brain slices. At first, the effect is characterised by an increasingly excitatory trend which is correlated with the increasing T14 concentration within the recording bath. This increase in neuronal output is halted (reaches a plateau) before being reversed at higher doses, an effect already reported using preparations as diverse as frog oocytes and organotypic tissue cultures (Greenfield et al., 2004). Additionally, the scrambled variant of the T14 (S14) showed an excitatory trend though never reaching significance: This result confirms that T14 effects observed were not due to the addition of a generic peptide and that these effects are sequence-specific. A minor query could be that the lower purity (>90%) of the S14 peptide compared to that of the T14 (>99%), in some way accounted for the differential findings of the two compounds. However since no resulting effect were seen with the less pure S14, it is hard to see how impurity could account for the bioactivity.

In the more complex, meso-scale preparation used here however, the exact processes by which this biphasic, dose-dependent effect occurs remains unclear: such a preparation (neuronal assemblies *in vitro*) involves a great number of individual components and processes from hundreds of millions of neurons which give rise, directly or indirectly, to the overall output recorded with field potentials. Such a scenario may account for the increase in variation seen with LFP recordings, indicating that during T14 application, individual traces showed the same profile in response over time, but with an increasingly high variability in the magnitude of the observed changes. Local field potential recordings provide information about all neuronal components within the vicinity of the recording electrode tip, which remains extremely varied in the neocortex: it therefore follows that the magnitude of the response is dependent on the exact distribution of neuronal types and their interconnectivity, which may be indirectly affected by the peptide during each individual experiment. This variation in neuronal circuitry may therefore be the result of different densities and/or localisation of neurons in addition to their sensitivity to T14 effects. Interestingly, after the initial excitatory trend seen with T14 application, a reverse, inhibitory trend is observed which may also be the result of a delayed, complex physiological antagonism on cortical networks.

Another factor helping to explain this increase in response variability over time is the distribution of target receptors through which T14 exerts its effects. T14 peptide significantly potentiates cation currents (and in particular: calcium, Ca^{2+}) through α_7-nAChRs (Zbarsky et al., 2004), which are among the most potent calcium ionophores – to a greater degree than NMDA receptors and other nAChR subtypes (Seguela et al., 1993). This mechanism is further modulated by the inhibition of these same calcium channels when the Ca^{2+} concentration reaches a critical level within cells (Standen and Stanfield, 1982). It follows therefore, that application of T14 would have a marked acute effect on neuronal output as well as more long-lasting, chronic effects as a result of excessive calcium influx into target neurons, possibly leading to cell death (for review, see: Berridge, 1998).

With regards to calcium-mediated calcium channel inactivation as a result of excessive Ca^{2+} entry within neurons, such an outcome may well have been achieved in our experiments as the T14 peptide was not only perfused in high concentrations (>1 μM) but also during extended periods of time: slices were indeed perfused with increasing concentrations of T14 for 96 min (~1 h 40 min). Together, these conditions may explain why the initially excitatory trend shown by T14 application shows such a biphasic profile, where excessive peptide action leads to the shutting down of otherwise excitatory processes. The fact recovery towards baseline-level is seen during washout condition supports this conclusion – as the T14 concentration drops, there is less α_7-nAChR potentiation which leads to less excessive Ca^{2+} currents entering neurons and reduced inactivation of those receptors.

4.3. T14 action at neuronal α_7-nAChRs

Methyllycaconitine (MLA) was used as a selective and competitive α_7-nAChR antagonist to assess the magnitude of T14 effects mediated by this receptor. It is not yet fully understood how AChE-related peptides precisely interact with the receptor, which includes one main ligand-binding site ('orthosteric' sites – where ACh binds) as well as at least one other allosteric site (where cholinergic modulators bind) per α_7 subunit (Wallace and Porter, 2011; Young et al., 2008). Previous work, however, has already shown that interacting with these allosteric binding sites has a significant effect on the binding of ligands at other sites, most probably by affecting receptor native conformation, and therefore the affinity of ligands for the binding sites (Bond et al., 2006; Greenfield et al., 2004; Onganer et al., 2006). In agreement with these earlier findings in more reductionist preparations, the effects of MLA perfusion in this study showed a prevention of the effects of T14 as well as reducing the extent to which the magnitude of the S.E.M increases (as seen during T14 perfusion alone, Fig. 1C). In order to confirm this effect was due to blockade of nicotinic receptors by MLA, and not to a simply high dose of the peptide alone (as discussed previously), the perfusion order was reversed such that MLA was applied for 32 min before the perfusion solution was switched to T14 for a further 32 min. In this case, no effect at all was seen as a result of the subsequent T14 perfusion (Fig. 2C) suggesting that MLA produced long-lasting effects which prevented T14 from successfully interacting with α_7-nAChRs. This effect may be explained by the rather large and complex structure of MLA which is equivalent to that of a small peptide (molecular weight: 682 g/mol; T14 molecular weight: 1864 g/mol) as well as its higher

affinity for the α_7-nAChR compared to that of the T14 peptide. In turn this similarity in molecular weight may account for why it takes up to 20 min for MLA to reverse the effects of the initial T14 perfusion, as well as validating the inefficacy of T14 after MLA perfusion. It is very probable that MLA would remain trapped within the slices' extracellular matrix where it would preferentially bind to α_7-nAChRs instead of T14 due to its higher affinity for the receptor. Taken together, these data confirm that the main effects induced by T14 perfusion can be effectively blocked using MLA, further implicating α_7-nAChR in mediating its acute effects on neuronal populations.

4.4. Comparison of data using electrophysiology vs optical imaging

Optical imaging using the fluorescent dye Di-4-ANEPPS was used to characterise further the actions of the T14 on neuronal signalling. VSDI revealed that the acute effects of T14 application on cortical networks produced differential patterns of activation: the perfusion of 0.7 μM T14 on cortical networks showed an increase in the time-course of activation while spread and intensity of activation remained unaffected. This increase in the time-course of activity as a result of 0.7 μM T14 application is valuable as it corroborates the increase in activity seen with LFP over time, but not over space. Activation intensity and spread were non-significantly altered under this particular condition. Similarly, none of the drug treatments perfused in this study affected the spread of neuronal activation, which shows that the excitability of neuronal networks was insignificantly affected by different drug treatments. However, when co-applied with MLA (in either order) data using optical imaging show a significant reduction in the intensity of activation, which in turn reflects a reduction in the synchrony of activation of neuronal populations, hence justifying the use of VSDI.

The two different techniques may well be expected to reveal complementary information. Di-4-ANEPPS, is a voltage-sensitive dye known to potentiate $GABA_A$ receptors (Mennerick et al., 2010), increasing the overall inhibitory component within slices. This off-target effect of Di-4-ANEPPS may explain further how excitation was reduced (T14 treatment) and inhibition increased (T14 and MLA co-perfusions) compared to field potential recordings. In addition, it is worthwhile noting that Di-4-ANEPPS, in particular, has been shown to stain preferentially the neuropil rather than cell soma: such work has been performed by imaging rat brain slices stained with Di-4-ANEPPS and imaged using two-photon laser scanning fluorescence microscopy (Denk et al., 1990; Yuste et al., 1997). Using this technique, it is possible to produce high-resolution imaging of micro-structures (such as dendritic trees and single-cell soma) located within highly light-scattering media, such as the neocortex (Denk et al., 1990). Research undertaken using this strategy to identify the structures which Di-4-ANEPPS stains preferentially, has confirmed that Di-4-ANEPPS stains structures within the neuropil rather than staining cell soma and primary dendrites (Yuste et al., 1997). Therefore, the results seen here with VSDI most accurately reflect changes in activity of the neuropil, where most of the processes and cortical computations take place, and where the effects of the peptide will be more potent, due to a higher area, a smaller cross section and possibly a higher receptor density. By contrast, LFP recordings do not discriminate and display changes in activity from all neuronal components (including cell soma). In turn this difference may explain why VSDI effects show a more pronounced inhibitory effect than LFP recordings.

In the presence of MLA, no increase in overall neuronal output by T14 is seen with either VSDI or LFP, confirming that potentiation of α_7-nAChR is halted upon MLA application. Furthermore, inhibitory effects seen only with VSDI when both MLA and T14 were co-applied also suggest an additive inhibitory effect as a result of the application of these agents. One possible hypothesis for this synergy may be that the T14 peptide and MLA bind at different sites on α_7-nAChR and, together, induce a more potent blockade of the receptor. Another possible hypothesis may be that secondary indirect effects within the complex neuronal circuitry from these two drugs produce a physiological antagonism which overall produces a net decrease in neuronal output.

4.5. Conclusion

Combining the data provided by LFP and VSDI in the present study, T14 was found to be bioactive in modulating neuronal activity from *in vitro* brain slice preparation (i.e. meso-scale 'neuronal assemblies'). T14 increased the output of cortical networks as revealed with LFP, while VSDI data showed it to increase the time-course of meso-scale neuronal activation. Furthermore, LFP recordings showed MLA reversed the excitatory effects of T14, through direct antagonism of α_7-nAChRs; while VSDI recordings not only showed a preferential effect of T14 and MLA within the neuropil rather than cell soma but also that significant inhibition was only induced when T14 and MLA were applied simultaneously, reducing the activation synchrony of neuronal populations. Hence this study provides further insight into the pharmacological actions of C-terminus AChE-related peptide on the holistic neuronal dynamics at the meso-scale level of cortical organisation. Such findings shed more light on a possible pivotal molecule in neurodegeneration by providing an early-stage mechanistic account of how such a peptide fragment could potentially trigger longer-term neurodegenerative processes.

Acknowledgements

The authors would like to thank the Mind Science Foundation and the Templeton Foundation for providing the funds to undertake this research. Special thanks must also go to Dr. Sara Garcia-Ratés, Dr. Ranya Bechara and Dr. Gwenael Pottiez for their valuable help in structuring, proofreading and editing the figures within this manuscript. Any corresponding communication should be addressed to Mr. Scott Badin, University of Oxford, Department of Pharmacology, Mansfield Road, Oxford, OX1 3QT. Tel: (+44) 01865 271626. E-mail: scott.badin@seh.ox.ac.uk

Appendix A. Supplementary data

Supplementary data related to this article can be found at http://dx.doi.org/10.1016/j.neuropharm.2013.05.019.

References

Aarsland, D., Tandberg, E., et al., 1996. Frequency of dementia in Parkinson disease. Arch. Neurol. 53 (6), 538–542.
Arendt, T., Bruckner, M.K., et al., 1992. Changes in acetylcholinesterase and butyrylcholinesterase in Alzheimer's disease resemble embryonic development – a study of molecular forms. Neurochem. Int. 21 (3), 381–396.
Berridge, M.J., 1998. Neuronal calcium signaling. Neuron 21 (1), 13–26.
Bon, C.L., Greenfield, S.A., 2003. Bioactivity of a peptide derived from acetylcholinesterase: electrophysiological characterization in guinea-pig hippocampus. Eur. J. Neurosci. 17 (9), 1991–1995.
Bond, C.E., Greenfield, S.A., 2007. Multiple cascade effects of oxidative stress on astroglia. Glia 55 (13), 1348–1361.
Bond, C.E., Patel, P., et al., 2006. Astroglia up-regulate transcription and secretion of 'readthrough' acetylcholinesterase following oxidative stress. Eur. J. Neurosci. 24 (2), 381–386.
Collins, T.F., Mann, E.O., et al., 2007. Dynamics of neuronal assemblies are modulated by anaesthetics but not analgesics. Eur. J. Anaesthesiol. 24 (7), 609–614.
Day, T., Greenfield, S.A., 2004. Bioactivity of a peptide derived from acetylcholinesterase in hippocampal organotypic cultures. Exp. Brain Res. 155 (4), 500–508.

DeKosky, S.T., 2001. Epidemiology and pathophysiology of Alzheimer's disease. Clin. Cornerstone 3 (4), 15–26.
Denk, W., Strickler, J.H., et al., 1990. Two-photon laser scanning fluorescence microscopy. Science 248 (4951), 73–76.
Devonshire, I.M., Dommett, E.J., et al., 2010a. Environmental enrichment differentially modifies specific components of sensory-evoked activity in rat barrel cortex as revealed by simultaneous electrophysiological recordings and optical imaging in vivo. Neuroscience 170 (2), 662–669.
Devonshire, I.M., Grandy, T.H., et al., 2010b. Effects of urethane anaesthesia on sensory processing in the rat barrel cortex revealed by combined optical imaging and electrophysiology. Eur. J. Neurosci. 32 (5), 786–797.
Emmett, S.R., Greenfield, S.A., 2004. A peptide derived from the C-terminal region of acetylcholinesterase modulates extracellular concentrations of acetylcholinesterase in the rat substantia nigra. Neurosci. Lett. 358 (3), 210–214.
Garcia-Rates, S., Lewis, M., et al., 2013. Additive toxicity of beta-amyloid by a novel bioactive peptide in vitro: possible implications for Alzheimer's disease. PLoS One 8 (2), e54864.
Gearing, M., Mirra, S.S., et al., 1995. The Consortium to Establish a Registry for Alzheimer's Disease (CERAD). Part X. Neuropathology confirmation of the clinical diagnosis of Alzheimer's disease. Neurology 45 (3 Pt 1), 461–466.
Gould, E., Woolf, N.J., et al., 1991. Postnatal-development of cholinergic neurons in the rat. 1. Forebrain. Brain Res. Bull. 27 (6), 767–789.
Greenfield, S., Vaux, D.J., 2002. Parkinson's disease, Alzheimer's disease and motor neurone disease: identifying a common mechanism. Neuroscience 113 (3), 485–492.
Greenfield, S.A., Day, T., et al., 2004. A novel peptide modulates alpha 7 nicotinic receptor responses: implications for a possible trophic-toxic mechanism within the brain. J. Neurochem. 90 (2), 325–331.
Greenfield, S.A., Zimmermann, M., et al., 2008. Non-hydrolytic functions of acetylcholinesterase. The significance of C-terminal peptides. FEBS J. 275 (4), 604–611.
Hof, P.R., Morrison, J.H., 2004. The aging brain: morphomolecular senescence of cortical circuits. Trends Neurosci. 27 (10), 607–613.
Hulette, C., Mirra, S., et al., 1995. The Consortium to Establish a Registry for Alzheimer's Disease (CERAD). Part IX. A prospective cliniconeuropathologic study of Parkinson's features in Alzheimer's disease. Neurology 45 (11), 1991–1995.
Lahiri, D.K., Chen, D., et al., 2007. The experimental Alzheimer's disease drug posiphen [(+)-phenserine] lowers amyloid-beta peptide levels in cell culture and mice. J. Pharmacol. Exp. Ther. 320 (1), 386–396.
Lahiri, D.K., Farlow, M.R., et al., 1998. The secretion of amyloid beta-peptides is inhibited in the tacrine-treated human neuroblastoma cells. Brain Res. Mol. Brain Res. 62 (2), 131–140.
Lahiri, D.K., Lewis, S., et al., 1994. Tacrine alters the secretion of the beta-amyloid precursor protein in cell lines. J. Neurosci. Res. 37 (6), 777–787.
Ling, J.J., Yu, J., et al., 1995. Sustained inhibition of acetylcholinesterase activity does not disrupt early geniculocortical ingrowth to developing rat visual cortex. Brain Res. Dev. Brain Res. 86 (1–2), 354–358.
Massoulie, J., Anselmet, A., et al., 1999. The polymorphism of acetylcholinesterase: post-translational processing, quaternary associations and localization. Chem. Biol. Interact. 119–120, 29–42.
Mennerick, S., Chisari, M., et al., 2010. Diverse voltage-sensitive dyes modulate GABA(A) receptor function. J. Neurosci. 30 (8), 2871–2879.
Morrison, J.H., Hof, P.R., 1997. Life and death of neurons in the aging brain. Science 278 (5337), 412–419.
Narr, K.L., Toga, A.W., et al., 2005. Cortical thinning in cingulate and occipital cortices in first episode schizophrenia. Biol. Psychiatry 58 (1), 32–40.
Oh, J.D., Butcher, L.L., et al., 1991. Thyroid-hormone modulates the development of cholinergic terminal fields in the rat forebrain – relation to nerve growth-factor receptor. Dev. Brain Res. 59 (2), 133–142.
Onganer, P.U., Djamgoz, M.B., et al., 2006. An acetylcholinesterase-derived peptide inhibits endocytic membrane activity in a human metastatic breast cancer cell line. Biochim. Biophys. Acta 1760 (3), 415–420.
Pohanka, M., 2011. Cholinesterases, a target of pharmacology and toxicology. Biomed. Pap. Med. Fac. Univ. Palacky Olomouc Czech Repub. 155 (3), 219–229.
Robertson, R.T., Yu, J., 1993. Acetylcholinesterase and neural development – new tricks for an old dog. News Physiol. Sci. 8, 266–272.
Rossor, M.N., 1981. Parkinson's disease and Alzheimer's disease as disorders of the isodendritic core. Br. Med. J. (Clin Res. Ed.) 283 (6306), 1588–1590.
Scahill, R.I., Schott, J.M., et al., 2002. Mapping the evolution of regional atrophy in Alzheimer's disease: unbiased analysis of fluid-registered serial MRI. Proc. Natl. Acad. Sci. U. S. A. 99 (7), 4703–4707.
Scarpini, E., Scheltens, P., et al., 2003. Treatment of Alzheimer's disease: current status and new perspectives. Lancet Neurol. 2 (9), 539–547.
Seguela, P., Wadiche, J., et al., 1993. Molecular-cloning, functional-properties, and distribution of rat brain-alpha-7-a nicotinic cation channel highly permeable to calcium. J. Neurosci. 13 (2), 596–604.
Shaw, K.T., Utsuki, T., et al., 2001. Phenserine regulates translation of beta-amyloid precursor protein mRNA by a putative interleukin-1 responsive element, a target for drug development. Proc. Natl. Acad. Sci. U. S. A. 98 (13), 7605–7610.
Shaw, P., Kabani, N.J., et al., 2008. Neurodevelopmental trajectories of the human cerebral cortex. J. Neurosci. 28 (14), 3586–3594.
Soreq, H., Seidman, S., 2001. Acetylcholinesterase – new roles for an old actor. Nat. Rev. Neurosci. 2 (4), 294–302.
Standen, N.B., Stanfield, P.R., 1982. A binding-site model for calcium-channel inactivation that depends on calcium entry. Proc. R. Soc. B-Biol. Sci. 217 (1206), 101–110.
Tominaga, T., Tominaga, Y., et al., 2000. Quantification of optical signals with electrophysiological signals in neural activities of Di-4-ANEPPS stained rat hippocampal slices. J. Neurosci. Methods 102 (1), 11–23.
Van De Werd, H.J., Uylings, H.B., 2008. The rat orbital and agranular insular prefrontal cortical areas: a cytoarchitectonic and chemoarchitectonic study. Brain Struct. Funct. 212 (5), 387–401.
Van Eden, C.G., Uylings, H.B., 1985. Cytoarchitectonic development of the prefrontal cortex in the rat. J. Comp. Neurol. 241 (3), 253–267.
Vickers, J.C., Dickson, T.C., et al., 2000. The cause of neuronal degeneration in Alzheimer's disease. Prog. Neurobiol. 60 (2), 139–165.
Wallace, T.L., Porter, R.H., 2011. Targeting the nicotinic alpha7 acetylcholine receptor to enhance cognition in disease. Biochem. Pharmacol. 82 (8), 891–903.
Webb, C.P., Nedergaard, S., et al., 1996. Involvement of the NMDA receptor in a non-cholinergic action of acetylcholinesterase in guinea-pig substantia nigra pars compacta neurons. Eur. J. Neurosci. 8 (4), 837–841.
Wlodarczyk, A., McMillan, P.F., et al., 2008. Voltage sensitive dye imaging of transient neuronal assemblies in brain slices under hyperbaric conditions. Undersea Hyperb. Med. 35 (1), 35–40.
Woolf, N.J., 1996. The critical role of cholinergic basal forebrain neurons in morphological change and memory encoding: a hypothesis. Neurobiol. Learn. Mem. 66 (3), 258–266.
Wu, J.Y., Huang, X., et al., 2008. Propagating waves of activity in the neocortex: what they are, what they do. Neuroscientist 14 (5), 487–502.
Young, G.T., Zwart, R., et al., 2008. Potentiation of alpha7 nicotinic acetylcholine receptors via an allosteric transmembrane site. Proc. Natl. Acad. Sci. U. S. A. 105 (38), 14686–14691.
Yuste, R., Tank, D.W., et al., 1997. Functional study of the rat cortical microcircuitry with voltage-sensitive dye imaging of neocortical slices. Cereb. Cortex 7 (6), 546–558.
Zbarsky, V., Thomas, J., et al., 2004. Bioactivity of a peptide derived from acetylcholinesterase: involvement of an ivermectin-sensitive site on the alpha 7 nicotinic receptor. Neurobiol. Dis. 16 (1), 283–289.